nature genetics

# Antagonistic roles of ubiquitin ligase HEI10 and SUMO ligase RNF212 regulate meiotic recombination

Huanyu Qiao[1,2], H B D Prasada Rao[1,2], Ye Yang[1,2], Jared H Fong[1,2], Jeffrey M Cloutier[3], Dekker C Deacon[3], Kathryn E Nagel[3], Rebecca K Swartz[3], Edward Strong[4], J Kim Holloway[5], Paula E Cohen[5], John Schimenti[4], Jeremy Ward[3] & Neil Hunter[1,2,6,7]



**Crossover recombination facilitates the accurate segregation of homologous chromosomes during meiosis[1,2]. In mammals, poorly characterized regulatory processes ensure that every pair of chromosomes obtains at least one crossover, even though most recombination sites yield non-crossovers[3]. Designation of crossovers involves selective localization of the SUMO ligase RNF212 to a minority of recombination sites, where it stabilizes pertinent factors such as MutSγ (ref. 4). Here we show that the ubiquitin ligase HEI10 (also called CCNB1IP1)[5,6] is essential for this crossover/non-crossover differentiation process. In HEI10-deficient mice, RNF212 localizes to most recombination sites, and dissociation of both RNF212 and MutSγ from chromosomes is blocked. Consequently, recombination is impeded, and crossing over fails. In wild-type mice, HEI10 accumulates at designated crossover sites, suggesting that it also has a late role in implementing crossing over. As with RNF212, dosage sensitivity for HEI10 indicates that it is a limiting factor for crossing over. We suggest that SUMO and ubiquitin have antagonistic roles during meiotic recombination that are balanced to effect differential stabilization of recombination factors at crossover and non-crossover sites.**

Variants in the *RNF212* and *CCNB1IP1* (*HEI10*) genes are associated with heritable variation in the rate of crossing over in humans[7–10]. The encoded RNF212 and HEI10 proteins also have structural and functional similarities. Both proteins have tripartite structures, with RING, coiled-coil and tail domains, and are inferred to catalyze post-translational protein modification by ubiquitin-like proteins[4–6,11,12]. RNF212 is implicated as an E3 enzyme for SUMO modification, whereas HEI10 has ubiquitin ligase activity (refs. 4,5,11 and Y.Y. and N.H., unpublished observation). In both *Hei10*$^{mei4/mei4}$ and *Rnf212*$^{-/-}$ mutant mice, early stages of meiosis occur normally, and full synapsis of homologous chromosomes (homologs) is achieved[4,6] (*mei4* is an allele of *Ccnb1ip1*, also known as *Hei10*). However, crossover-specific recombination complexes, containing the MutLγ complex (MLH1 and MLH3) and cyclin-dependent kinase CDK2, do not assemble[4,6]. Consequently, crossing over fails, and the mice are sterile. These similarities prompted us to examine the relationship between these two pro-crossover factors.

Using immunofluorescence cytology, we previously described the dynamic localization of RNF212 to synaptonemal complexes[4], the meiosis-specific structures that connect homologs along their lengths during the pachytene stage of meiosis. As homologs undergo synapsis during zygonema, RNF212 localizes specifically to the central region of synaptonemal complexes, forming a punctate pattern of immunostaining foci. Consistent with previous analysis[4], in wild-type spermatocytes at early pachynema, when synapsis is complete, we observed ~150 foci per nucleus (**Fig. 1a**,**k**). By midpachynema, most staining had disappeared, and RNF212 foci were retained only at sites where crossovers form (**Fig. 1b**,**c**,**k**). These crossover-specific RNF212 foci were then lost by late pachynema, before the disassembly of synaptonemal complexes at diplonema (**Fig. 1d**,**e**,**k**).

In spermatocytes from *Hei10*$^{mei4/mei4}$ mice, the early staining pattern of abundant RNF212 foci appeared normal (155.9 ± 37.2 (s.d.) foci, 20 early pachytene nuclei versus 153.0 ± 42.8 foci in wild-type spermatocytes, 20 nuclei; **Fig. 1f**,**k**). Strikingly, this pattern persisted throughout pachynema, and loss of RNF212 from the chromosomes was only seen when synaptonemal complexes were disassembled during diplonema (**Fig. 1g**–**k**). Moreover, the numbers of RNF212 foci were significantly higher than ever seen in wild-type spermatocytes ($P$ = 0.0003, Mann-Whitney test). Thus, HEI10 is required for the turnover of RNF212 after synapsis that culminates in its selective retention at future crossover sites.

To examine the consequences of persistent RNF212 for recombination in *Hei10*$^{mei4/mei4}$ mutants, we examined the chromosomal dynamics of the MutSγ complex (**Fig. 2**). MutSγ comprises MSH4 and MSH5, two meiosis-specific homologs of the bacterial DNA mismatch-binding factor MutS[13]. Published studies indicate that MutSγ binds and stabilizes DNA strand-exchange intermediates to

[1]Howard Hughes Medical Institute, University of California, Davis, Davis, California, USA. [2]Department of Microbiology & Molecular Genetics, University of California, Davis, Davis, California, USA. [3]Department of Biology, Middlebury College, Middlebury, Vermont, USA. [4]Department of Molecular Biology & Genetics, Cornell University College of Veterinary Medicine, Ithaca, New York, USA. [5]Center for Reproductive Genomics, Department of Biomedical Sciences, Cornell University, Ithaca, New York, USA. [6]Department of Molecular & Cellular Biology, University of California, Davis, Davis, California, USA. [7]Department of Cell Biology & Human Anatomy, University of California, Davis, Davis, California, USA. Correspondence should be addressed to N.H. (nhunter@ucdavis.edu).

Received 12 June 2013; accepted 4 December 2013; published online 5 January 2014; doi:10.1038/ng.2858

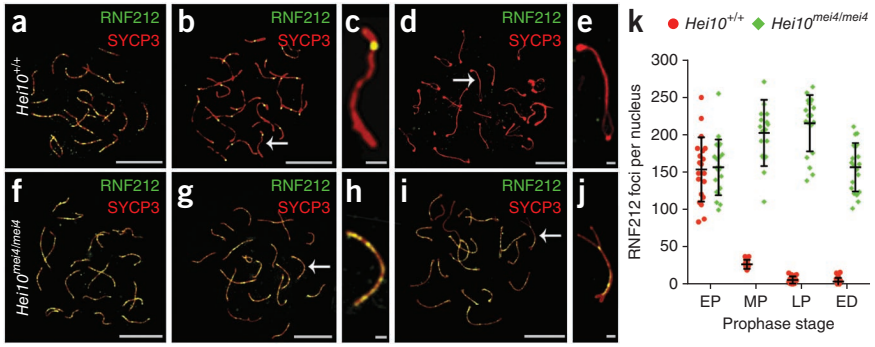


**Figure 1** RNF212 does not dissociate from synaptonemal complexes in *Hei10* $^{mei4/mei4}$ mutant spermatocytes. All nuclei were immunostained for RNF212 (green) and homolog axis component SYCP3 (red). (**a**–**e**) Wild-type (*Hei10*$^{+/+}$) nuclei at early pachynema (**a**), midpachynema (**b**,**c**) and early diplonema (**d**,**e**). **c** and **e** show magnified views of the chromosomes indicated by arrows in **b** and **d**, respectively. (**f**–**j**) *Hei10*$^{mei4/mei4}$ mutant nuclei at early pachynema (**f**), midpachynema (**g**,**h**) and early diplonema (**i**,**j**). **h** and **j** show magnified views of the chromosomes indicated by arrows in **g** and **j**, respectively. (**k**) Quantification of RNF212 foci (± s.d.) at successive prophase I stages. EP, early pachynema; MP, midpachynema; LP, late pachynema; ED, early diplonema. Twenty nuclei were analyzed for each stage. Scale bars, 10 μm in **a**,**b**,**d**,**f**,**g**,**i** and 1 μm in **c**,**e**,**h**,**j**.

promote both homolog synapsis and crossing over[14,15]. We previously showed[4] that a minority of MutSγ foci present in early pachynema colocalize with RNF212. Analysis of *Rnf212*$^{-/-}$ mice indicated that RNF212 acts to stabilize MutSγ and thereby designate a crossover fate to this subset of recombination sites.

Here we confirmed that the chromosomal localization of MutSγ in wild-type spermatocytes resembled that of RNF212: specifically, 82.9 ± 23.4 (s.d.) MSH4 immunostaining foci were observed in late zygonema and early pachynema, whereas at midpachynema only 39.4 ± 9.6 foci were retained, and MSH4 staining had essentially disappeared by the onset of diplonema (**Fig. 2a**–**e**,**k**). In *Hei10*$^{mei4/mei4}$ mutant spermatocytes, the chromosomal dynamics of MutSγ were severely aberrant. Although normal numbers of MSH4 foci were formed at late zygonema/early pachynema, focus numbers remained high throughout pachynema and only decreased after homologs desynapsed at diplonema (**Fig. 2f**–**k**).

Super-resolution structured illumination microscopy (SIM)[16] showed that the stabilization of MutSγ foci correlated with the degree of colocalization of MutSγ and RNF212 (**Fig. 2l**–**p** and **Supplementary Fig. 1**). Consistent with our previous analysis[4], around a third of MSH4 foci colocalized with RNF212 in late-zygotene and early pachytene spermatocytes (**Fig. 2l**,**m**,**p** and **Supplementary Fig. 1**). In sharp contrast, in *Hei10*$^{mei4/mei4}$ mutant spermatocytes, MSH4 foci showed a high level of colocalization (~90%) with RNF212 foci at all

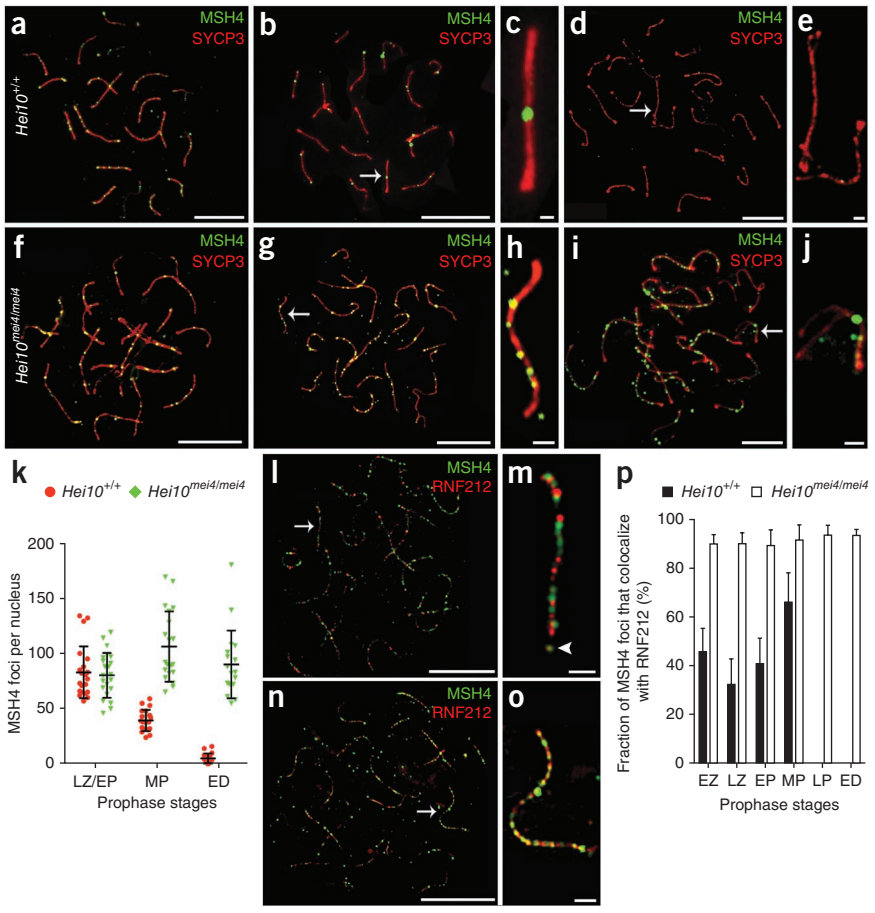


**Figure 2** Persistence of MutSγ complexes in *Hei10*$^{mei4/mei4}$ spermatocytes. (**a**–**j**) Spermatocyte nuclei immunostained for MSH4 (green) and SYCP3 (red). (**a**–**e**) Wild-type nuclei at late zygonema (**a**), midpachynema (**b**,**c**) and early diplonema (**d**,**e**). **c** and **e** show magnified views of the chromosomes indicated by arrows in **b** and **d**, respectively. (**f**–**j**) *Hei10*$^{mei4/mei4}$ mutant nuclei at late zygonema (**f**), midpachynema (**g**,**h**) and early diplonema (**i**,**j**). **h** and **j** show magnified views of the chromosomes indicated by arrows in **g** and **i**, respectively. (**k**) Quantification of MSH4 foci (± s.d.) at successive prophase I stages. Numbers of nuclei analyzed at late zygonema/early pachynema (LZ/EP), midpachynema (MP) and early diplonema (ED), respectively: 21, 20 and 20 for *Hei10*$^{+/+}$ spermatocytes and 21, 20 and 18 for *Hei10*$^{mei4/mei4}$ spermatocytes. (**l**–**o**) SIM images of early pachytene nuclei immunostained for MSH4 (green) and RNF212 (red). To allow accurate staging, nuclei were also stained for SYCP3 (data not shown). (**l**) Wild-type nucleus. (**m**) Magnification of the chromosome highlighted by the arrow in **l**. (**n**) *Hei10*$^{mei4/mei4}$ mutant nucleus. (**o**) Magnification of the chromosome highlighted by the arrow in **n**. (**p**) Percentage of MSH4 foci (± s.d.) that colocalize with RNF212 foci at successive prophase substages determined by SIM analysis. Numbers of *Hei10*$^{+/+}$ nuclei analyzed at early zygonema (EZ), late zygonema (LZ), early pachynema (EP) and midpachynema (MP), respectively: 10, 5, 10 and 7. Numbers of *Hei10*$^{mei4/mei4}$ nuclei analyzed at early zygonema (EZ), late zygonema (LZ), early pachynema (EP), midpachynema (MP), late pachynema (LP) and early diplonema (ED), respectively: 5, 6, 25, 14, 9 and 9. Scale bars, 10 μm in **a**,**b**,**d**,**f**,**g**,**i**,**l**,**n** and 1 μm in **c**,**e**,**h**,**j**,**m**,**o**.

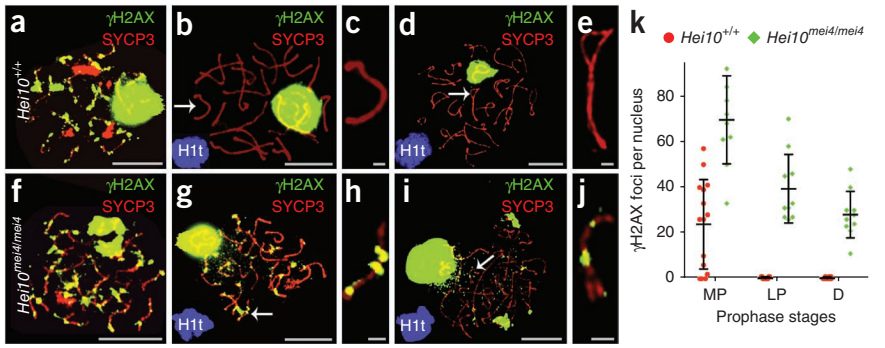


**Figure 3** Repair of DSBs is delayed in *Hei10*$^{mei4/mei4}$ spermatocytes. All nuclei were immunostained for γH2AX (green), SYCP3 (red) and the histone variant H1t (shown as blue insets in **b**,**d**,**g**,**i**). The latter marks prophase nuclei that have progressed beyond early pachynema and is used to facilitate substaging of pachynema nuclei. (**a**–**e**) Wild-type nuclei at early pachynema (**a**), midpachynema (**b**,**c**) and diplonema (**d**,**e**). **c** and **e** show magnified views of the chromosomes indicated by arrows in **b** and **d**, respectively. (**f**–**j**) *Hei10*$^{mei4/mei4}$ mutant nuclei at early pachynema (**f**), midpachynema (**g**,**h**) and early diplonema (**i**,**j**). **h** and **j** show magnified views of the chromosomes indicated by arrows in **g** and **i**, respectively. (**k**) Quantification of γH2AX foci (± s.d.) at successive prophase I stages. Numbers of nuclei analyzed at midpachynema (MP), late pachynema (LP) and diplonema (D), respectively: 15, 11 and 10 for *Hei10*$^{+/+}$ and 10, 10 and 10 for *Hei10*$^{mei4/mei4}$. Scale bars, 10 μm in **a**,**b**,**d**,**f**,**g**,**i** and 1 μm in **c**,**e**,**h**,**j**.

stages from early zygonema through early diplonema (**Fig. 2n**–**p** and **Supplementary Fig. 1**). These observations lend further support to our inference that RNF212 stabilizes the association of MutSγ with recombination sites[4]. Thus, RNF212 and HEI10 have antagonistic functions with respect to the stabilization of MutSγ at recombination sites. We suggest that the balance of their two activities underpins the temporal dynamics and spatial patterning of RNF212 and MutSγ seen in wild-type spermatocytes.

Meiotic recombination is initiated by the programed formation of DNA double-strand breaks (DSBs)[15]. The persistence of MutSγ complexes implies that DSB repair is delayed in *Hei10*$^{mei4/mei4}$ spermatocytes. Immunostaining for DSB-induced H2AX phosphorylation (γH2AX) supported this inference (**Fig. 3**). In wild-type nuclei, γH2AX staining initially formed a pan-nuclear cloud, which diminished to limited chromatin flares and foci as chromosome synapsis ensued and finally disappeared from autosomes around midpachynema[17] (**Fig. 3a**–**e**,**k**; note that γH2AX accumulated as a large staining body on the chromatin of the sex chromosomes, where it facilitates transcriptional silencing[18]). In *Hei10*$^{mei4/mei4}$ spermatocytes, although pan-nuclear γH2AX staining diminished with synapsis, delayed DSB repair was indicated by the persistence of γH2AX foci throughout pachynema (**Fig. 3f**–**j**,**k**). Ultimately, however, DSBs appear to be repaired in *Hei10*$^{mei4/mei4}$ spermatocytes, as broken chromatids are not detected in late-stage nuclei[6]. Together, these data suggest that HEI10-dependent elimination of RNF212 from synaptonemal complexes is required for the timely removal of MutSγ from most recombination sites as pachynema progresses. This in turn allows the timely progression of recombination and the repair of DSBs.

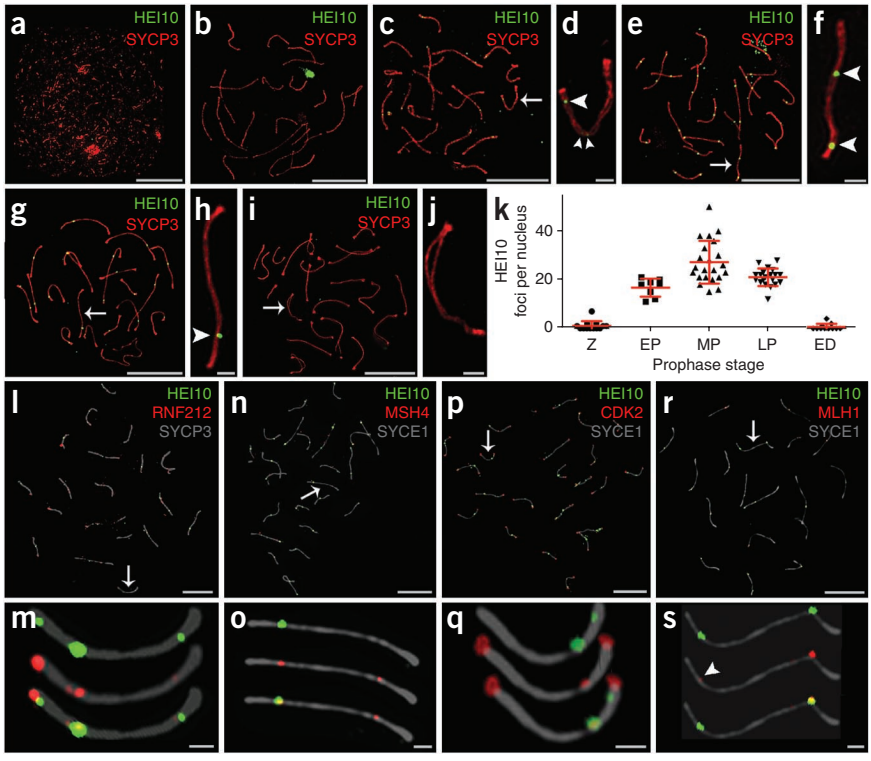


**Figure 4** HEI10 localization to synaptonemal complexes and crossover sites. (**a**–**j**) Representative SIM images of wild-type spermatocyte nuclei immunostained for HEI10 (green) and SYCP3 (red) at leptonema (**a**), late zygonema (**b**), early pachynema (**c**,**d**), midpachynema (**e**,**f**), late pachynema (**g**,**h**) and early diplonema (**i**,**j**). **d**, **f**, **h** and **j** show magnified views of the chromosomes indicated by arrows in **c**, **e**, **g** and **i**, respectively. Arrowheads highlight HEI10 foci. (**k**) Numbers of HEI10 foci per nucleus at successive prophase stages. Horizontal bars represent means ± s.d. Numbers of nuclei analyzed at zygonema (Z), early pachynema (EP), midpachynema (MP), late pachynema (LP) and early diplonema (ED), respectively: 13, 8, 22, 20 and 11. (**l**,**m**) Midpachytene spermatocyte immunostained for HEI10 (green), RNF212 (red) and SYCP3 (gray). **m** shows a magnified view of the chromosome indicated by the arrow in **l**. (**n**,**o**) Midpachytene spermatocyte immunostained for HEI10 (green), MSH4 (red) and synaptonemal complex central element protein SYCE1 (gray). **o** shows a magnified view of the chromosome indicated by the arrow in **n**. (**p**,**q**) Midpachytene spermatocyte immunostained for HEI10 (green), CDK2 (red) and SYCE1 (gray). **q** shows a magnified view of the chromosome indicated by the arrow in **p**. (**r**,**s**) Midpachytene spermatocyte immunostained for HEI10 (green), MLH1 (red) and SYCE1 (gray). **s** shows a magnified view of the chromosome indicated by the arrow in **r**. The arrowhead highlights a small MLH1 focus that colocalizes with HEI10. Scale bars, 10 μm in **a**–**c**,**e**,**g**,**i**,**l**,**n**,**p**,**r** and 1 μm in **d**,**f**,**h**,**j**,**m**,**o**,**q**,**s**.

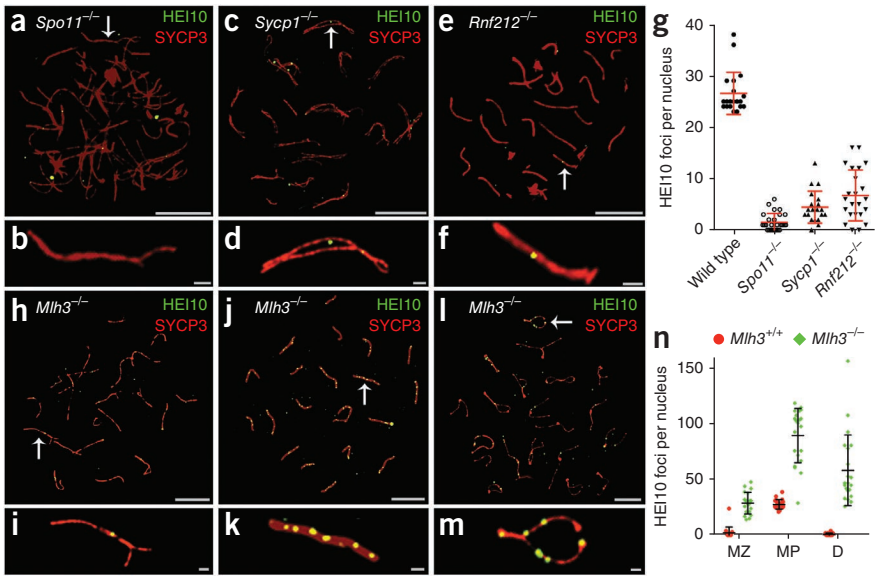


**Figure 5** Genetic requirements for HEI10 localization. (**a**–**m**) Representative spermatocyte nuclei, from indicated mutant lines, immunostained for HEI10 (green) and SYCP3 (red). (**a**,**b**) Spermatocyte nucleus from a *Spo11*$^{-/-}$ mouse. **b** shows a magnification of the chromosome indicated by the arrow in **a**. (**c**,**d**) Spermatocyte nucleus from a *Sycp1*$^{-/-}$ mouse. **d** shows a magnification of the chromosome indicated by the arrow in **c**. (**e**,**f**) Spermatocyte nucleus from a *Rnf212*$^{-/-}$ mouse. **f** shows a magnification of the chromosome indicated by the arrow in **e**. (**g**) Numbers of HEI10 foci per nucleus in mid- to late-pachytene spermatocytes from wild-type, *Spo11*$^{-/-}$, *Sycp1*$^{-/-}$ and *Rnf212*$^{-/-}$ mice. Bars represent means ± s.d. Numbers of nuclei analyzed: wild-type, 20; *Spo11*$^{-/-}$, 27; *Sycp1*$^{-/-}$, 20; *Rnf212*$^{-/-}$, 23. Analysis of *Spo11*$^{-/-}$ nuclei was confined to those with high levels of synapsis, predicted to be the equivalents of midpachytene nuclei. Similarly, only *Sycp1*$^{-/-}$ nuclei with a high degree of pseudosynapsis were analyzed. However, true equivalents of wild-type midpachytene nuclei may not be represented in *Spo11*$^{-/-}$ and *Sycp1*$^{-/-}$ testes owing to apoptosis[18,20]. (**h**–**m**) Representative spermatocyte nuclei from *Mlh3*$^{-/-}$ mutant spermatocytes. (**h**) Late-zygotene nucleus. (**i**) Magnification of the chromosome indicated by the arrow in **h**. (**j**) Midpachytene nucleus. (**k**) Magnification of the chromosome indicated by the arrow in **j**. (**l**) Mid-diplotene nucleus. (**m**) Magnification of the chromosome indicated by the arrow in **l**. (**n**) Numbers of HEI10 foci per nucleus (± s.d.) at successive prophase stages in wild-type and *Mlh3*$^{-/-}$ mice. Number of nuclei analyzed at midzygonema (MZ), midpachynema (MP) and diplonema (D), respectively: 20, 22 and 20 for wild-type (*Mlh3*$^{+/+}$) spermatocytes and 20, 21 and 21 for *Mlh3*$^{-/-}$ spermatocytes. Scale bars, 10 μm in **a**,**c**,**e**,**h**,**j**,**l** and 1 μm in **b**,**d**,**f**,**i**,**k**,**m**.

Despite their broadly similar phenotypes, we can now conclude that *Rnf212*$^{-/-}$ and *Hei10*$^{mei4/mei4}$ mutants have distinct defects with respect to the designation of crossover sites. In the absence of RNF212, the designation of crossover sites fails because no MutSγ complexes are stabilized beyond early pachynema[4], whereas the absence of HEI10 causes most or all MutSγ complexes to be stabilized, as though all sites had been designated a crossover fate. These findings raise the following question: why do *Hei10*$^{mei4/mei4}$ mutants not form numerous crossovers?

Insights into this question, as well as into how HEI10 regulates the dynamics of RNF212 and MutSγ, came from examining the chromosomal localization pattern of HEI10. Although previous attempts to localize mouse HEI10 to meiotic chromosomes have been unsuccessful[6], we were able to show that mouse HEI10 associates with synaptonemal complexes to form distinct immunostaining foci (**Fig. 4a**–**k** and **Supplementary Figs. 2** and **3**). Unlike RNF212, distinct foci of HEI10 were rarely detected along nascent synaptonemal complexes during zygonema (**Fig. 4a**). Given that *Hei10*$^{mei4/mei4}$ phenotypes are already apparent at this time (for example, **Fig. 2p**), we infer that cytologically undetectable HEI10 regulates the early stage dynamics of RNF212 and MutSγ. Indeed, the possibility that this function of HEI10 does not involve association with meiotic chromosomes cannot be ruled out. However, by early pachynema, HEI10 foci could be detected (**Fig. 4c**,**d**), and their numbers peaked during midpachynema with an average of 27 foci per nucleus (27.2 ± 8.8 (s.d.) foci, 22 nuclei; **Fig. 4e**,**f**,**k**). At this stage, HEI10 focus numbers were quite variable, with as few as 15 and as many as 50 foci per nucleus. In late-pachytene nuclei, the average HEI10 focus number was lower and was less variable (21.1 ± 3.6 (s.d.) foci, 20 nuclei; **Fig. 4g**,**h**,**k**). At the onset of diplonema, HEI10 foci were no longer detected (**Fig. 4i**,**j**).

As HEI10 promotes loss of RNF212 and MutSγ from synaptonemal complexes, we examined the colocalization of these proteins (**Fig. 4l**–**o**). In midpachytene spermatocytes, only 23% of RNF212 foci and 29% of MSH4 foci colocalized with HEI10 (respectively, 22.6 ± 7.7% (s.d.) and 28.9 ± 15.1% foci, 10 nuclei each). HEI10 is required for the formation of crossover-specific complexes containing CDK2 and MutLγ (MLH1-MLH3). In contrast to what was observed for RNF212 and MSH4, a high degree of colocalization was seen for these markers and HEI10 (**Fig. 4p**–**s**): 74.0 ± 10.7% (s.d.) of non-telomeric CDK2 foci and 94.3 ± 6.9% of MLH1 foci colocalized with HEI10 (10 and 19 nuclei, respectively). These data are consistent with HEI10 foci superseding complexes of RNF212 and MutSγ at future crossover sites.

We investigated the genetic requirements for the chromosomal localization of HEI10 using several mutant lines (**Fig. 5**). SPO11 catalyzes DNA breakage to initiate recombination[15]. In *Spo11*$^{-/-}$ spermatocytes, homolog pairing is defective, but a substantial fraction of nuclei assemble incomplete synaptonemal complexes, which generally involve non-homologous chromosomes[19,20]. We found that the numbers of HEI10 foci were diminished, although foci were not completely eliminated, in these nuclei (**Fig. 5a**,**b**,**g**). This dependency contrasts that of RNF212, which readily associates with synaptonemal complexes independent of recombination[4].SYCP1 is a major component of the synaptonemal complex central region[21]. In *Sycp1*$^{-/-}$ mice, meiotic recombination initiates normally and homologs closely coalign, but synapsis is precluded. In addition, MutLγ foci are not detected in *Sycp1*$^{-/-}$ nuclei, indicating that the designation or maturation of crossover sites fails in this mutant. We found that the formation of HEI10 foci was greatly reduced in pachytene-like *Sycp1*$^{-/-}$ spermatocytes, but most nuclei contained a few foci (4.5 ± 3.1 (s.d.) foci per nucleus, 20 nuclei; **Fig. 5c**,**d**,**g**). In *Rnf212*$^{-/-}$ mutants, homologs undergo synapsis but the designation of crossover sites is defective[4]. As in the *Sycp1*$^{-/-}$ mutants, we observed that a few HEI10 foci were detected in *Rnf212*$^{-/-}$ mutant spermatocytes (6.7 ± 4.9 (s.d.) foci, 23 nuclei; **Fig. 5e**–**g**). We infer that the initiation of recombination, homolog synapsis and the designation of crossover sites are important for the normal formation and/or stabilization of HEI10 foci.

Finally, we examined HEI10 localization in mice lacking the MLH3 component of the crossover-specific factor MutLγ (ref. 13).

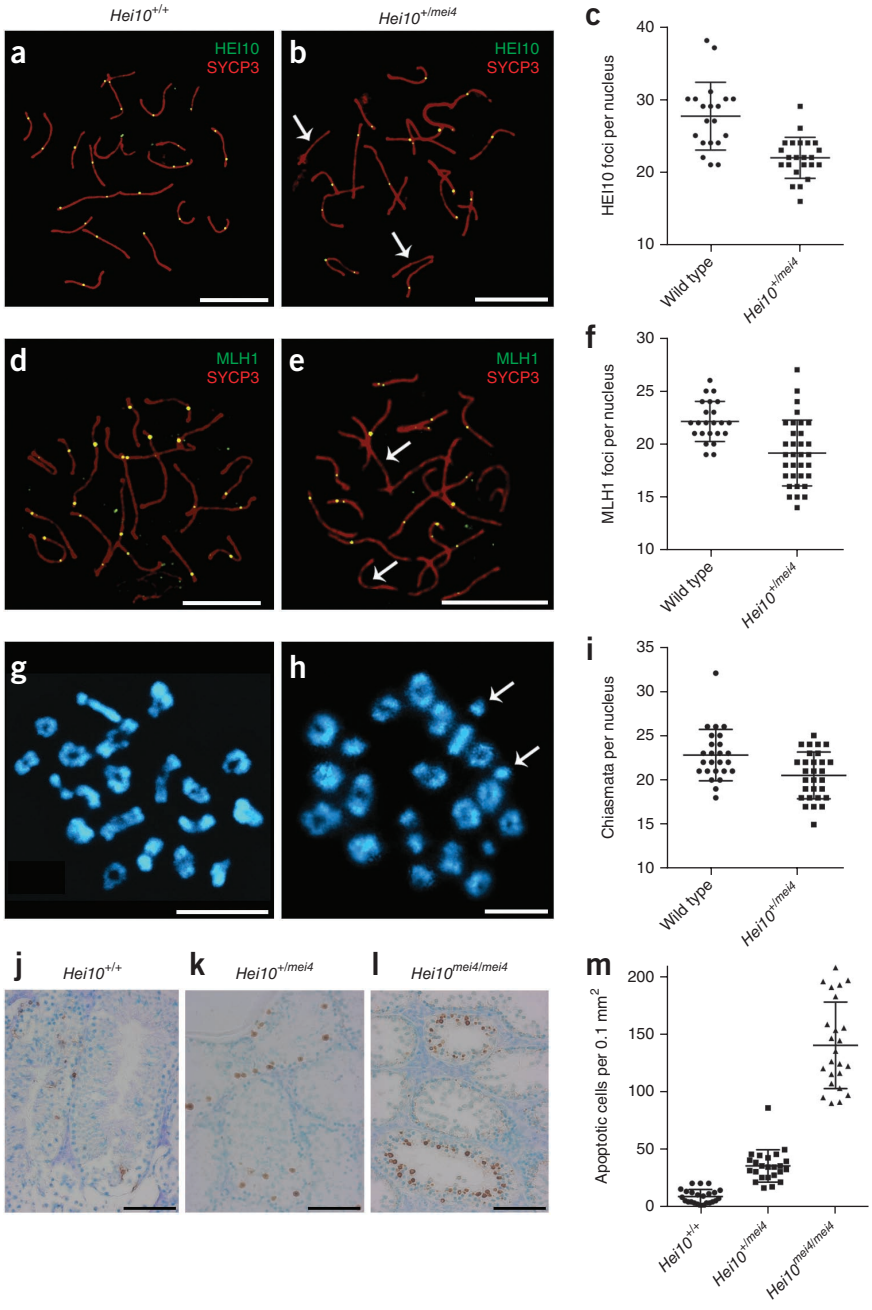


**Figure 6** Dosage sensitivity of the HEI10 crossover function. (**a**,**b**) Midpachytene nuclei from wild-type (*Hei10*$^{+/+}$) mice (**a**) and *Hei10*$^{+/mei4}$ heterozygous mice (**b**) immunostained for HEI10 (green) and SYCP3 (red). The arrows in **b** highlight chromosomes that lack HEI10 foci. (**c**) Numbers of HEI10 foci (± s.d.) per nucleus in midpachytene cells (23 wild-type and 33 *Hei10*$^{+/mei4}$ nuclei). (**d**,**e**) Midpachytene nuclei from wild-type mice (**d**) and *Hei10*$^{+/mei4}$ heterozygous mice (**e**) immunostained for MLH1 and SYCP3. The arrows in **e** highlight chromosomes that lack MLH1 foci. (**f**) Numbers of MLH1 foci per nucleus (± s.d.) in midpachytene cells (20 wild-type and 23 *Hei10*$^{+/mei4}$ nuclei). (**g**,**h**) Chromosome spreads of diakinesis/metaphase I spermatocytes from wild-type mice (**g**) and *Hei10*$^{+/mei4}$ heterozygous mice (**h**) stained with DAPI. (**i**) Numbers of chiasmata per nucleus (± s.d.) in diakinesis/metaphase I spermatocytes (25 wild-type and 29 *Hei10*$^{+/mei4}$ nuclei). (**j**–**l**) TUNEL-stained testis sections from *Hei10*$^{+/+}$ (**j**), *Hei10*$^{+/mei4}$ (**k**) and *Hei10*$^{mei4/mei4}$ (**l**) mice. (**m**) Quantification of TUNEL-positive apoptotic cells (± s.d.) in spermatocyte sections. Scale bars, 10 μm in **a**,**b**,**d**,**e**,**g**,**h** and 100 μm in **j**–**l**.

In *Mlh3*$^{-/-}$ spermatocytes, homolog synapsis and the initial designation of crossover sites appear normal, but the implementation of crossing over fails[4,22]. In sharp contrast to the other mutants we examined, high numbers of HEI10 foci were observed in *Mlh3*$^{-/-}$ spermatocytes (**Fig. 5h**–**m**). Unlike in wild-type mice, HEI10 foci were already detectable in zygonema (**Fig. 5h**,**i**,**n**), reached very high numbers during mid-pachynema (89.9 ± 24.5 (s.d.) foci per nucleus, 21 nuclei; **Fig. 5j**,**k**,**n**) and persisted into diplonema (**Fig. 5l**–**n**). At least half of the foci in midpachynema were coincident with γH2AX staining (53.0 ± 12.5% (s.d.) foci, 10 nuclei; **Supplementary Fig. 4**), implying that the majority of HEI10 accumulates at sites of DSB repair in *Mlh3*$^{-/-}$ cells.

These data suggest that the chromosomal localization of HEI10 occurs in two phases. First, HEI10 is licensed to accumulate into foci associated with synaptonemal complexes. These complexes, normally transient, may generally promote the progression of recombination. In wild-type cells, the relatively high and variable numbers of HEI10 foci seen in midpachynema may be a manifestation of this first phase. Subsequently, stable accumulation of HEI10 specifically at crossover sites is directed by MLH3 (and presumably by MLH1). Notably, MLH3 restrains accumulation of HEI10 during zygonema, an early function that was not anticipated from the timing of crossover-specific MLH3 foci, which do not appear until early to mid-pachynema[13].

Taken together, our data imply that HEI10 functions during zygonema to limit the colocalization of RNF212 with MutSγ-associated recombination sites and thereby establish early differentiation of crossover and non-crossover sites. Later, HEI10 is directed by MutLγ (and perhaps by CDK2) to stably accumulate at designated crossover sites. Here we propose that HEI10 also promotes the dissociation of RNF212 and MutSγ to allow the progression of recombination and the implementation of the final steps of crossing over. The model in **Supplementary Figure 5** synthesizes the key points of our analysis and those of previous studies.

Recently, recombination rate in humans has been associated with a variant in the 5′ UTR of *CNNB1IP1* (*HEI10*)[10] that has the potential to alter expression levels, suggesting that HEI10 may be a dosage-sensitive regulator of crossing over. To determine whether the crossover function of mouse HEI10 is dosage sensitive, we analyzed spermatocytes from *Hei10*$^{+/mei4}$ heterozygotes (**Fig. 6**). Indeed, significant decreases in the numbers of HEI10 foci (20.6%), MLH1 foci (13.5%) and chiasmata (10%) were detected ($P = 0.0003$, $P < 0.0001$ and $P = 0.0088$, respectively, Mann-Whitney test). In spermatocytes, homologs not tethered by crossovers are detected by the spindle checkpoint, which triggers apoptosis[23]. Consistent with the reduced crossing over seen in *Hei10*$^{+/mei4}$ heterozygotes, we detected a significant increase in

the number of apoptotic (TUNEL-positive) cells in testes sections from *Hei10*$^{+/mei4}$ heterozygotes ($P < 0.0001$, Mann-Whitney test; **Fig. 6j–m** and **Supplementary Fig. 6**).

Intriguingly, the crossover function of RNF212 also shows dosage sensitivity in the mouse, and human *RNF212* variants have been associated with changes in recombination rate[4,7–9]. These observations are consistent with the idea that a balance between SUMO and ubiquitin is a key aspect of crossover regulation. It will be interesting to see whether human alleles of *CNNB1IP1* (*HEI10*), *RNF212* and genes encoding recombination factors such as MutSγ interact to modulate recombination rate, fertility and the risk of aneuploidy.

## METHODS

Methods and any associated references are available in the online version of the paper.

*Note: Any Supplementary Information and Source Data files are available in the online version of the paper.*

### ACKNOWLEDGMENTS

We thank A. Kong for communicating unpublished results. This work was supported by US National Institutes of Health (NIH) grants R01GM084955 to N.H., R01GM45415 to J.S. and HD041012 to P.E.C. and by National Science Foundation grant CAREER 0844941 to J.W. N.H. is an investigator of the Howard Hughes Medical Institute.

### AUTHOR CONTRIBUTIONS

H.Q., H.B.D.P.R., Y.Y., J.W. and N.H. conceived and designed the experiments. H.Q., H.B.D.P.R., Y.Y., J.H.F., J.M.C., D.C.D., K.E.N., R.K.S., E.S., J.K.H., J.W. and N.H. performed the experiments. H.Q., H.B.D.P.R., Y.Y., J.H.F., J.W. and N.H. analyzed the data. J.S., E.S. and P.E.C. contributed reagents, materials and/or analysis tools. H.Q., H.B.D.P.R., Y.Y., J.W. and N.H. wrote the manuscript.

### COMPETING FINANCIAL INTERESTS

The authors declare no competing financial interests.



1. Sakuno, T., Tanaka, K., Hauf, S. & Watanabe, Y. Repositioning of aurora B promoted by chiasmata ensures sister chromatid mono-orientation in meiosis I. *Dev. Cell* **21**, 534–545 (2011).
2. Hirose, Y. *et al.* Chiasmata promote monopolar attachment of sister chromatids and their co-segregation toward the proper pole during meiosis I. *PLoS Genet.* **7**, e1001329 (2011).
3. Jones, G.H. The control of chiasma distribution. *Symp. Soc. Exp. Biol.* **38**, 293–320 (1984).
4. Reynolds, A. *et al.* RNF212 is a dosage-sensitive regulator of crossing-over during mammalian meiosis. *Nat. Genet.* **45**, 269–278 (2013).
5. Toby, G.G., Gherraby, W., Coleman, T.R. & Golemis, E.A. A novel RING finger protein, human enhancer of invasion 10, alters mitotic progression through regulation of cyclin B levels. *Mol. Cell Biol.* **23**, 2109–2122 (2003).
6. Ward, J.O. *et al.* Mutation in mouse *hei10*, an e3 ubiquitin ligase, disrupts meiotic crossing over. *PLoS Genet.* **3**, e139 (2007).
7. Kong, A. *et al.* Sequence variants in the *RNF212* gene associate with genome-wide recombination rate. *Science* **319**, 1398–1401 (2008).
8. Fledel-Alon, A. *et al.* Variation in human recombination rates and its genetic determinants. *PLoS ONE* **6**, e20321 (2011).
9. Chowdhury, R., Bois, P.R., Feingold, E., Sherman, S.L. & Cheung, V.G. Genetic analysis of variation in human meiotic recombination. *PLoS Genet.* **5**, e1000648 (2009).
10. Kong, A. *et al.* Common and low-frequency variants associated with genome-wide recombination rate. *Nat. Genet.* **46**, 11–16 (2014).
11. Cheng, C.H. *et al.* SUMO modifications control assembly of synaptonemal complex and polycomplex in meiosis of *Saccharomyces cerevisiae*. *Genes Dev.* **20**, 2067–2081 (2006).
12. Strong, E.R. & Schimenti, J.C. Evidence implicating CCNB1IP1, a RING domain–containing protein required for meiotic crossing over in mice, as an E3 SUMO ligase. *Genes (Basel)* **1**, 440–451 (2010).
13. Kolas, N.K. & Cohen, P.E. Novel and diverse functions of the DNA mismatch repair family in mammalian meiosis and recombination. *Cytogenet. Genome Res.* **107**, 216–231 (2004).
14. Snowden, T., Acharya, S., Butz, C., Berardini, M. & Fishel, R. hMSH4-hMSH5 recognizes Holliday junctions and forms a meiosis-specific sliding clamp that embraces homologous chromosomes. *Mol. Cell* **15**, 437–451 (2004).
15. Hunter, N. in *Molecular Genetics of Recombination* (eds. Aguilera, A. & Rothstein, R.) 381–442 (Springer-Verlag, Heidelberg, 2006).
16. Carlton, P.M. Three-dimensional structured illumination microscopy and its application to chromosome structure. *Chromosome Res.* **16**, 351–365 (2008).
17. Chicheportiche, A., Bernardino-Sgherri, J., de Massy, B. & Dutrillaux, B. Characterization of Spo11-dependent and independent phospho-H2AX foci during meiotic prophase I in the male mouse. *J. Cell Sci.* **120**, 1733–1742 (2007).
18. Fernandez-Capetillo, O. *et al.* H2AX is required for chromatin remodeling and inactivation of sex chromosomes in male mouse meiosis. *Dev. Cell* **4**, 497–508 (2003).
19. Baudat, F., Manova, K., Yuen, J.P., Jasin, M. & Keeney, S. Chromosome synapsis defects and sexually dimorphic meiotic progression in mice lacking Spo11. *Mol. Cell* **6**, 989–998 (2000).
20. Romanienko, P.J. & Camerini-Otero, R.D. The mouse *Spo11* gene is required for meiotic chromosome synapsis. *Mol. Cell* **6**, 975–987 (2000).
21. de Vries, F.A. *et al.* Mouse Sycp1 functions in synaptonemal complex assembly, meiotic recombination, and XY body formation. *Genes Dev.* **19**, 1376–1389 (2005).
22. Lipkin, S.M. *et al.* Meiotic arrest and aneuploidy in MLH3-deficient mice. *Nat. Genet.* **31**, 385–390 (2002).
23. Eaker, S., Cobb, J., Pyle, A. & Handel, M.A. Meiotic prophase abnormalities and metaphase cell death in MLH1-deficient mouse spermatocytes: insights into regulation of spermatogenic progress. *Dev. Biol.* **249**, 85–95 (2002).

## ONLINE METHODS

**Mice.** All mice were congenic with the C57BL/6J background. Mice were maintained and used for experimentation according to the guidelines of the Institutional Animal Care and Use Committees of the University of California, Davis, and the Middlebury College Animal Facility. The *Hei10*, *Mlh3*, *Rnf212*, *Spo11* and *Sycp1* mutant lines and primer sequences for genotyping were previously described[4,6,19,21,22]. Male mice between 2–6 months of age were used for experimentation.

**Protein blot analysis.** Tissues from adult mice were sonicated in RIPA buffer, protein concentration was measured by the Bradford assay, and 100–200 μg of protein was separated by SDS-PAGE. After protein transfer to nitrocellulose membranes (Waterman), blots were incubated overnight with the following antibodies: mouse monoclonal antibody to CCNB1IP1/HEI10 (ab118999, Abcam; 1:2,000 dilution), rabbit polyclonal antibody to CCNB1IP1/HEI10 (this study; 1:2,000 dilution) or mouse antibody to tubulin (BioLegend, 625902; 1:2,000 dilution). Secondary antibodies (1:10,000 dilution) were goat antibody to rabbit or mouse IgG conjugated to horseradish peroxidase (HRP; SouthernBiotech, 4050-05 and 1031-05, respectively). HRP was detected using ECL reagent (Pierce).

**Antibody production.** A polyclonal antibody against mouse HEI10/CCNB1IP1 was raised in rabbits against a mixture of two C-terminal peptides. Antibodies were purified from serum using Protein A/G spin columns (GE Healthcare). Antibody specificity was determined by protein blotting and immunofluorescence staining of material from wild-type and *Hei10*$^{mei4/mei4}$ mice.

**Cytology.** Testes and ovaries were dissected from freshly killed mice and processed for surface spreading as described[24]. Sample size was determined empirically; for all quantification, images from at least two mice ($n$ = 2–5) were analyzed. Comparisons were made between mice that were either littermates or were matched by age. All cytological analyses were performed by two observers; the second observer was blinded to which group or genotype was being analyzed. Immunofluorescence staining was performed as described[25] using the following primary antibodies with incubation overnight at room temperature: mouse antibody to SYCP3 (sc-74568, Santa Cruz Biotechnology; 1:200 dilution), rabbit antibody to SYCP3 (sc-33195, Santa Cruz Biotechnology; 1:300 dilution), guinea pig antibody to SYCE1 (1:2,000 dilution) (generously provided by C. Höög, Karolinska Institutet)[26], guinea pig antibody to RNF212 (1:50 dilution)[4], rabbit antibody to RNF212 (1:200 dilution)[4], rabbit antibody to MSH4 (ab58666, Abcam; 1:100 dilution), mouse monoclonal antibody to CCNB1IP1/HEI10 (ab118999, Abcam; 1:150 dilution), rabbit polyclonal antibody to CCNB1IP1/HEI10 (this study), mouse antibody to MLH1 (550838, BD Pharmingen; 1:50 dilution), mouse monoclonal antibody to γH2AX (05-636, Millipore; 1:500 dilution), mouse monoclonal antibody to CDK2 (sc-6248, Santa Cruz Biotechnology; 1:200 dilution) and guinea pig antibody to H1t (a gift from M.A. Handel, Jackson Laboratory; 1:1,000 dilution)[27]. Slides were subsequently incubated with the following goat secondary antibodies for 1 h at 37 °C: anti-rabbit 488 (A11070, Molecular Probes; 1:1,000 dilution), anti-rabbit 568 (A11036, Molecular Probes; 1:2,000 dilution), anti-mouse 555 (A21425, Molecular Probes; 1:1,000 dilution), anti-mouse 594 (A11020, Molecular Probes; 1:1,000 dilution), anti-mouse 488 (A11029, Molecular Probes; 1:1,000 dilution) and anti–guinea pig fluorescein isothiocyanate (106-096-006 FITC, Jackson Labs; 1:200 dilution). Coverslips were mounted with ProLong Gold antifade reagent (Molecular Probes). For chiasma counts, air-dried preparations of cells in diakinesis/metaphase I were prepared as described[28] and stained with DAPI.

**TUNEL assays.** Testes were fixed in formalin, embedded in paraffin, sectioned and processed using the ApopTag Plus Peroxidase *In Situ* Apoptosis Detection kit (Chemicon).

**Imaging.** Immunolabeled chromosome spreads and DAPI-stained diakinesis/metaphase I nuclei were imaged using a Zeiss AxioPlan II microscope with a 63× Plan Apochromat 1.4 objective and an EXFO X-Cite metal halide light source. Images were captured by a Hamamatsu ORCA-ER CCD camera and processed using the Volocity (Perkin Elmer) and Photoshop (Adobe) software packages. SIM analysis was performed using a Nikon N-SIM super-resolution microscope system and NIS-Elements 2 image-processing software. MSH4-RNF212 colocalization was determined using NIS-Elements, and cofoci were confirmed by visual inspection. Testes sections were imaged using an Axiovert 200 microscope and AxioCamMRc camera with AxioVision 4.4 software. Apoptotic cells were imaged and counted in representative fields of view.


24. Holloway, J.K., Booth, J., Edelmann, W., McGowan, C.H. & Cohen, P.E. MUS81 generates a subset of MLH1-MLH3–independent crossovers in mammalian meiosis. *PLoS Genet.* **4**, e1000186 (2008).
25. Qiao, H., Lohmiller, L. & Anderson, L. Cohesin proteins load sequentially during prophase I in tomato primary microsporocytes. *Chromosome Res.* **19**, 193–207 (2011).
26. Costa, Y. *et al.* Two novel proteins recruited by synaptonemal complex protein 1 (SYCP1) are at the centre of meiosis. *J. Cell Sci.* **118**, 2755–2762 (2005).
27. Cobb, J., Cargile, B. & Handel, M.A. Acquisition of competence to condense metaphase I chromosomes during spermatogenesis. *Dev. Biol.* **205**, 49–64 (1999).
28. Holloway, J.K., Morelli, M.A., Borst, P.L. & Cohen, P.E. Mammalian BLM helicase is critical for integrating multiple pathways of meiotic recombination. *J. Cell Biol.* **188**, 779–789 (2010).

# Antagonistic roles of ubiquitin ligase HEI10 and SUMO ligase RNF212 regulate meiotic recombination.

Huanyu Qiao, H.B.D. Prasada Rao, Ye Yang, Jared H. Fong, Jeffrey M. Cloutier, Dekker C. Deacon, Kathryn E. Nagel, Rebecca K. Swartz, Edward Strong, J. Kim Holloway, Paula E. Cohen, John Schimenti, Jeremy Ward & Neil Hunter

**Supplementary Information**

**Six Figures**



Nature Genetics: doi:10.1038/ng.2858

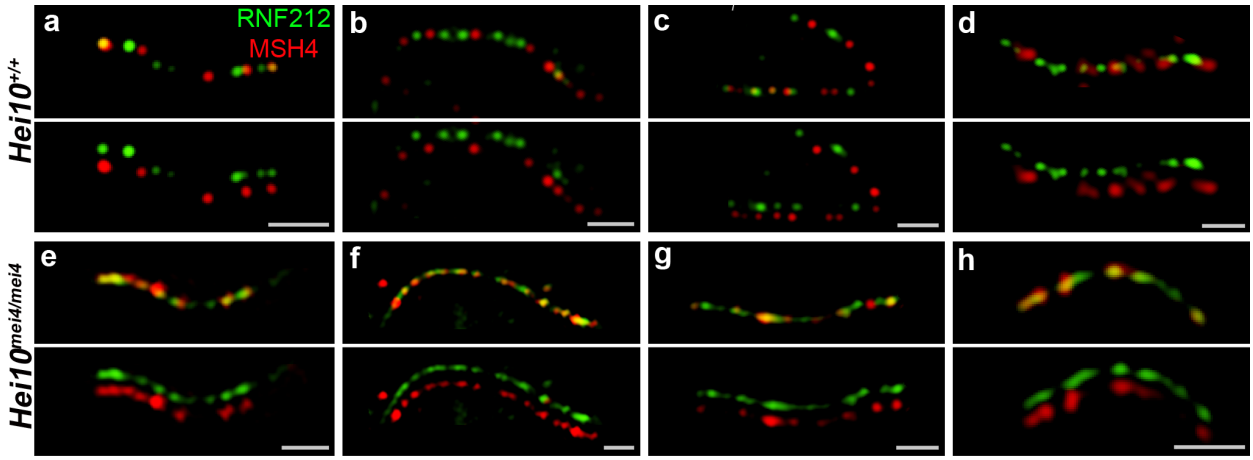


**Supplementary Figure 1** SIM analysis of RNF212-MSH4 colocalization in early pachynema. Chromosome spreads from wild-type and *Hei10*$^{mei4/mei4}$ spermatocytes were immunostained for MSH4 (red) and RNF212 (green) and imaged by SIM. To allow accurate staging, nuclei were also stained for SYCP3 (not shown). (**a-d**) Selected chromosomes from wild-type nuclei. In the top panels the MSH4 and RNF212 channels are merged. In the lower panels, the two channels are offset horizontally to highlight foci that are aligned. (**e-h**) Selected chromosomes from *Hei10*$^{mei4/mei4}$ nuclei.



Nature Genetics: doi:10.1038/ng.2858

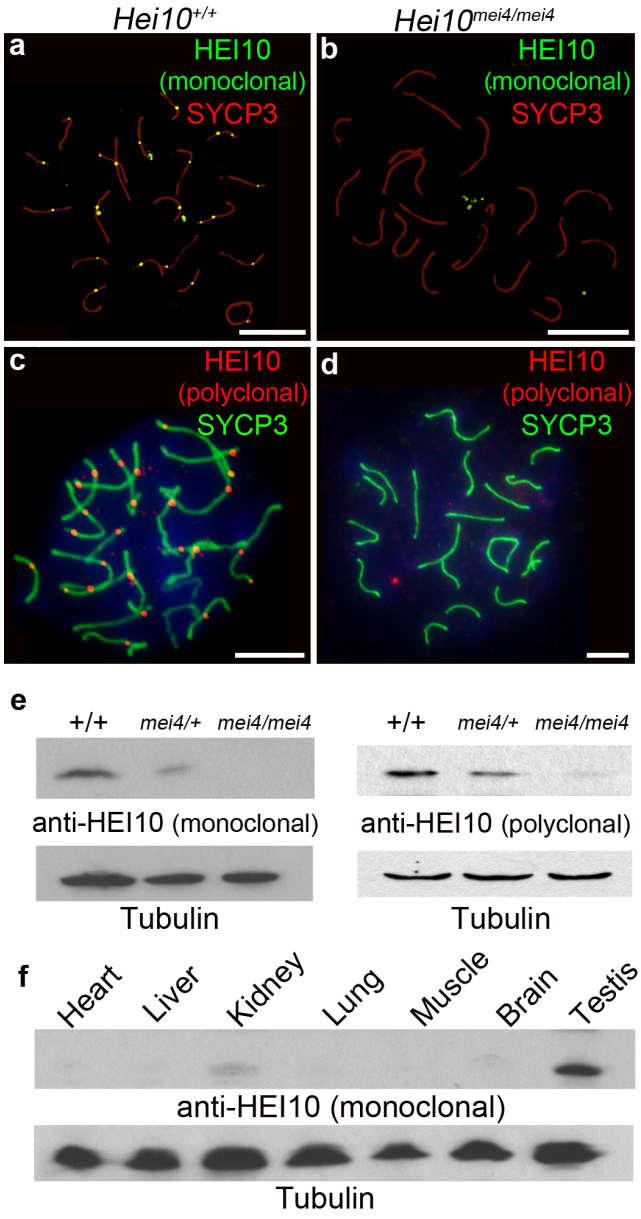


**Supplementary Figure 2** Characterization of HEI10/CNNB1IP1 antibodies.

(**a–d**) Spermatocyte nuclei from wild-type (**a,c**) and *Hei10*$^{mei4/mei4}$ (**b,d**) mice immunostained for HEI10 and SYCP3. Mouse monoclonal and rabbit polyclonal anti-HEI10 antibodies were used in **a,b** and **c,d**, respectively. The nuclei in **c,d** are also counterstained with DAPI. Scale bars are 10 μm. (**e**) Protein blot analysis of HEI10 in testis cell extracts from wild-type, *Hei10*$^{+/mei4}$



Nature Genetics: doi:10.1038/ng.2858

heterozygous and *Hei10*$^{mei4/mei4}$ homozygous mice. The blot shown in the left panel was incubated with the mouse monoclonal anti-HEI10 antibody and the blot shown in right panel was incubated with rabbit anti-HEI10 polyclonal antibody. The *Hei10*$^{mei4}$ allele was predicted by Ward *et al.* to express an in-frame, 24 amino-acid deletion of HEI10 protein (252 vs. 276 amino acids)[6], but little if any protein is detected in *Hei10*$^{mei4/mei4}$ homozygotes and a shorter form is not apparent in *Hei10*$^{+/mei4}$ heterozygotes. However, protein blot analysis using polyclonal HEI10 antibodies (right panels) suggests that residual protein may remain in *Hei10*$^{mei4/mei4}$ homozygotes. (**f**) Protein blot analysis of extracts from various tissues using the mouse monoclonal anti-HEI10 antibody.

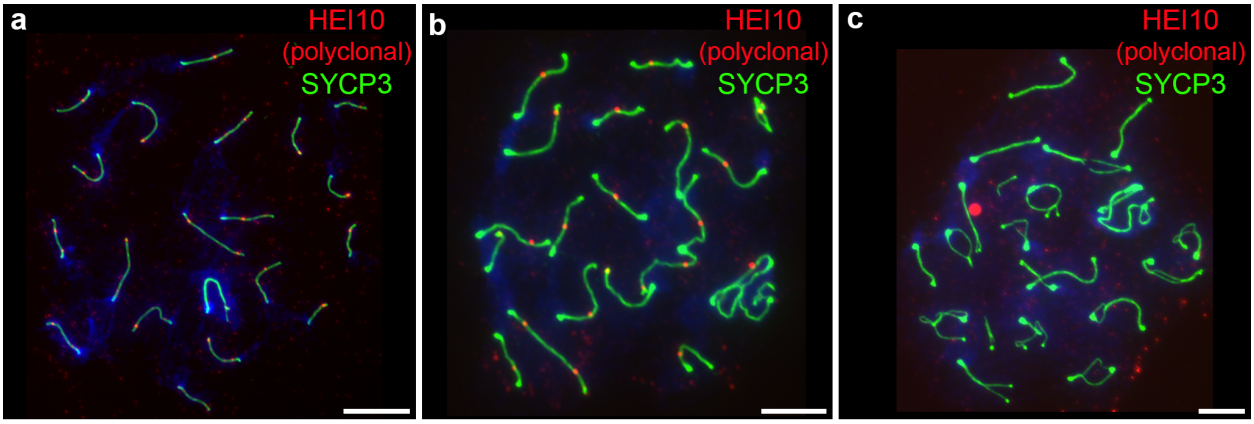


**Supplementary Figure 3** HEI10 foci detected with the rabbit polyclonal antibody. Representative wild-type spermatocytes immunostained for HEI10, using the rabbit polyclonal anti-HEI10 antibody (red), and SYCP3 (green) at mid pachynema (**a**), late pachynema (**b**), and early-mid diplonema (**c**). Nuclei are also counterstained with DAPI. In mid-pachynema, an average of 24.5 ± 3.4 (s.d.) foci per nucleus was detected (24 nuclei) using this antibody; 23.4 ± 3.3 foci were detected in late pachytene nuclei (10 nuclei).



Nature Genetics: doi:10.1038/ng.2858

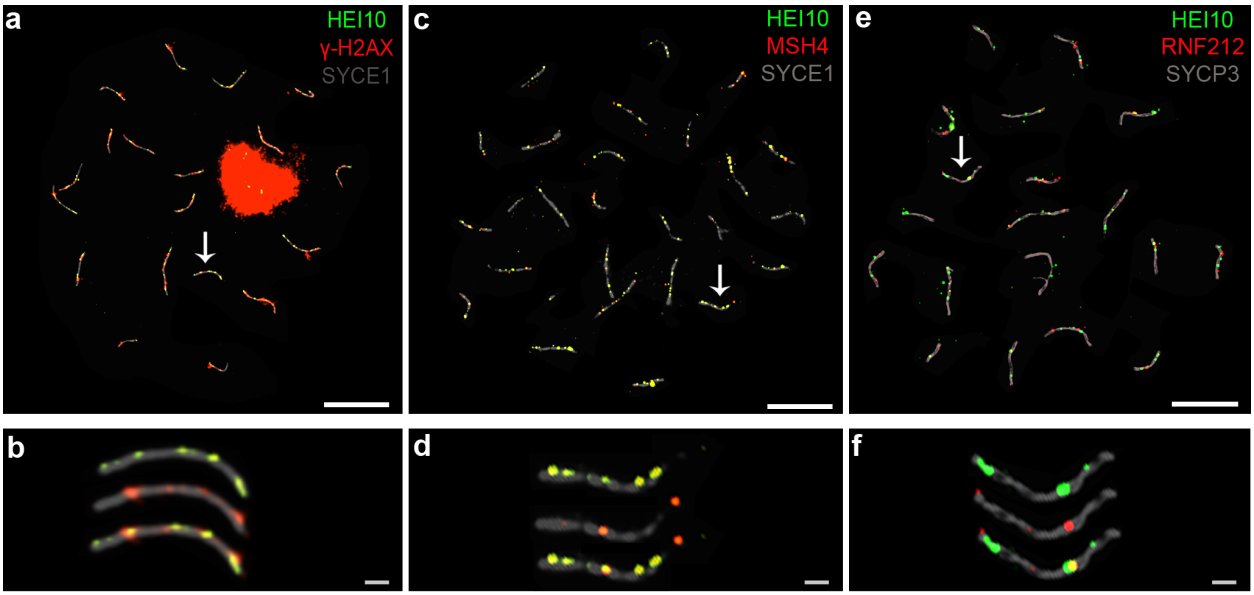


Scale bars are 10 μm.

**Supplementary Figure 4** Analysis of HEI10 foci in *Mlh3*$^{-/-}$ Spermatocytes.

(**a,b**) Mid-pachytene *Mlh3*$^{-/-}$ spermatocyte immunostained for HEI10 (green), γH2AX (red), and synaptonemal complex central element protein, SYCE1 (grey). (**b**) Magnified view of the chromosome indicated by the arrow in **a**. (**c,d**) Mid-pachytene *Mlh3*$^{-/-}$ spermatocyte immunostained for HEI10 (green), MSH4 (red) and SYCE1 (grey). (**d**) Magnified view of the chromosome indicated by the arrow in **c**. (**e,f**) Mid-pachytene *Mlh3*$^{-/-}$ spermatocyte immunostained for HEI10 (green), RNF212 (red), and SYCP3 (grey). (**f**) Magnified view of the chromosome indicated by the arrow in **e**.

Scale bars, 10 μm in **a, c, e,**; 1 μm in **b, d f.**

53.0 ± 12.5% (s.d., 10 nuclei) of HEI10 foci in mid pachytene cells were coincident with γH2AX staining. In contrast, only 18% ± 2.5% (s.d., 10 nuclei) of HEI10 foci colocalized with MSH4, but 46.6 ± 8.8% of MSH4 foci showed colocalization with HEI10. This difference is largely



Nature Genetics: doi:10.1038/ng.2858

explained by the disparity between the numbers of HEI10 and MSH4 foci at this stage (93.7 ± 11.3 (s.d.) and 37 ± 6.4, respectively). Similarly, 26.0 ± 5.8 (s.d., 10 nuclei) of HEI10 foci showed colocalization with RNF212 and 46.6% ± 11.1% of RNF212 foci were colocalized with HEI10. Thus, in *Mlh3*$^{-/-}$ spermatocytes at mid pachynema, HEI10 foci tend to be associated with sites marked by γH2AX, but not by MSH4 or RNF212. Unlike HEI10, the dynamics of MSH4 and RNF212 foci appear to be normal in *Mlh3*$^{-/-}$ spermatocytes. As such, they are outnumbered by HEI10 foci in mid pachynema cells.

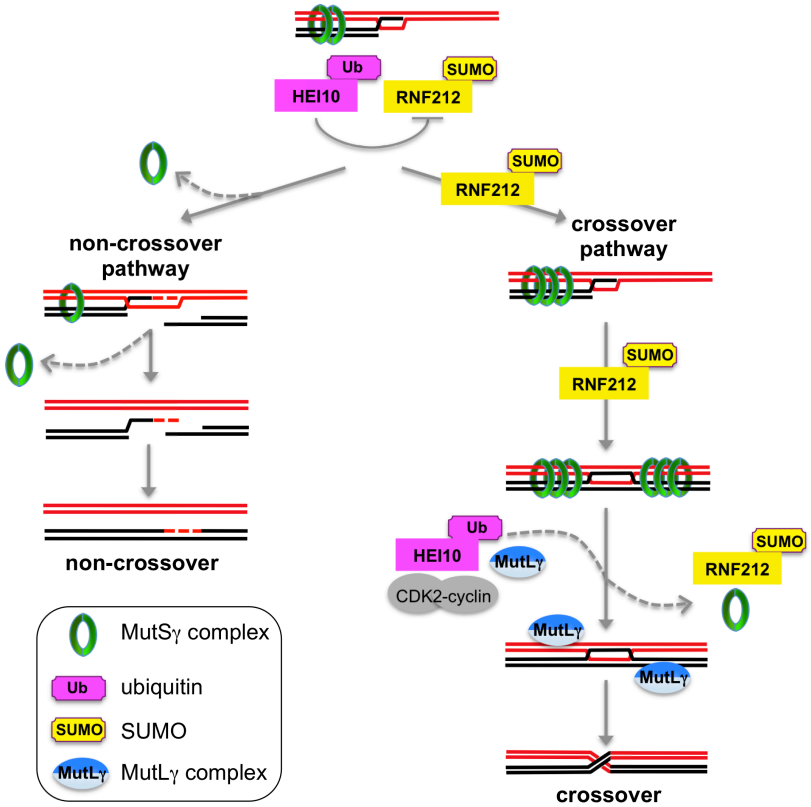


**Supplementary Figure 5** Model of HEI10 function.

MutSγ initially binds at most or all recombination (DSB) sites to stabilize nascent recombination intermediates and facilitate homolog synapsis[13,14]. The balance of HEI10-mediated ubiquitylation and RNF212-mediate SUMOylation then determines the post-synapsis stability of MutSγ-



Nature Genetics: doi:10.1038/ng.2858

associated recombination complexes. The relevant target proteins are currently unknown. "Winners" accumulate sufficient RNF212 to stabilize MutSγ, which facilitates formation of crossover-specific DNA intermediates (presumably double-Holliday Junctions[14]). In contrast, MutSγ dissociates from all other sites, allowing progression of recombination towards the default non-crossover outcome. At designated crossover sites, MutLγ directs or stabilizes accumulation of HEI10 where it acts to displace RNF212 and MutSγ, and allow the final steps of crossing over to be implemented.



Nature Genetics: doi:10.1038/ng.2858

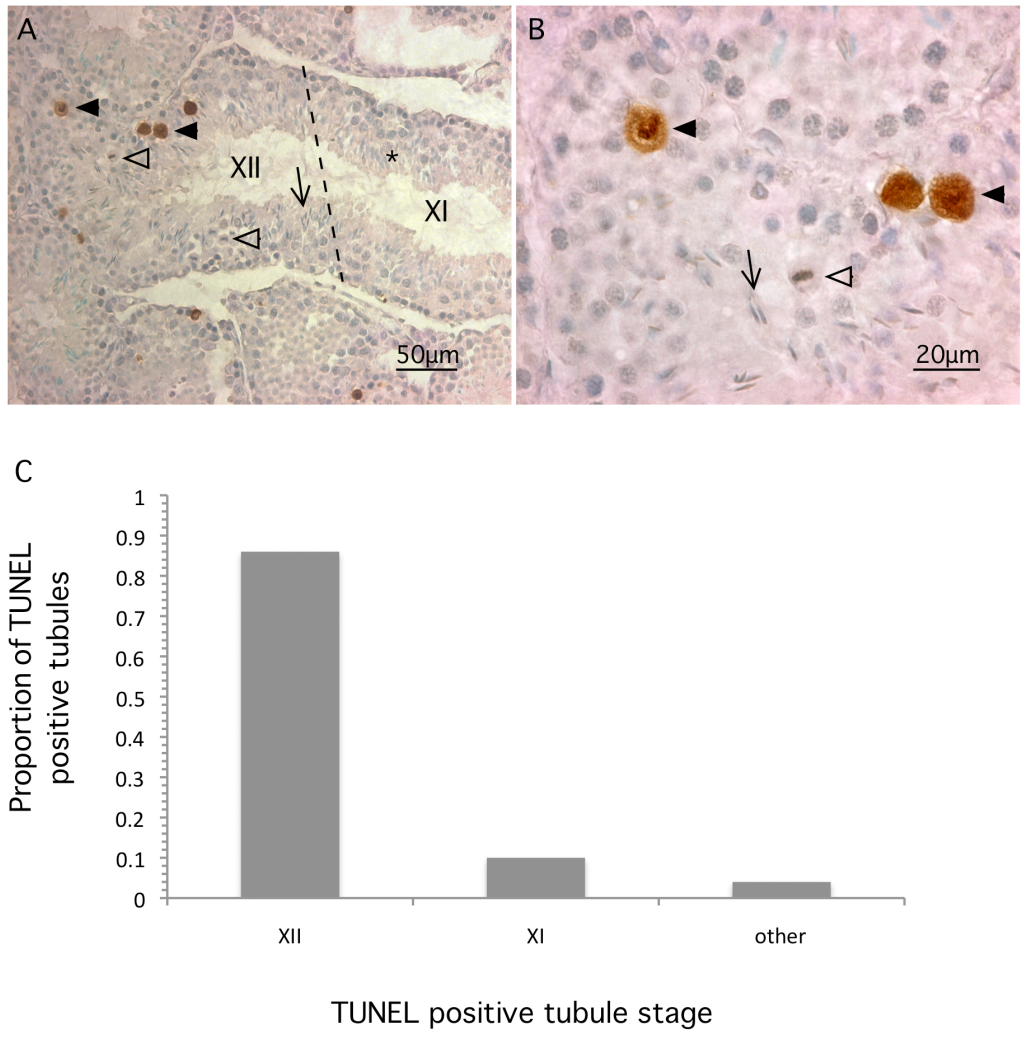


**Supplementary Figure 6** Apoptosis in *Hei10*$^{+/mei4}$ seminiferous tubules.

(**a**) Image of a long tubule section from a *Hei10*$^{+/mei4}$ heterozygote containing stages XII and XI. The presence of meiosis I cells (open arrowheads) and spermatids with long dense nuclei (arrow) are diagnostic of stage XII; these figures are absent in the adjacent stage XI tubule section, but variable elongated spermatid heads are present (indicated by an asterisk). Brown TUNEL-positive staining is only seen for metaphase cells in the stage XII tubule section (highlighted by black arrowheads). (**b**) Higher magnification image of the stage XII tubule section highlighting



Nature Genetics: doi:10.1038/ng.2858

the dense chromatin of a metaphase I cell and an elongated spermatid nucleus. (**c**) Graph showing the fractions of TUNEL-positive cells located in tubules at stages XII, XI or others (50 TUNEL-positive tubules from two *Hei10*$^{+/mei4}$ animals were analyzed).



Nature Genetics: doi:10.1038/ng.2858